



# A computational study on the adsorption and $\cdot\text{OH}$ initiated photochemical and photocatalytic primary oxidation of aniline

Hilal S. Wahab\*, Andreas D. Koutselos

Laboratory of Physical Chemistry, Chemistry Department, National and Kapodistrian University of Athens, Zografou 15771, Athens, Greece

## ARTICLE INFO

### Article history:

Received 26 July 2008

Accepted 30 January 2009

Available online 5 February 2009

### Keywords:

Adsorption

Aniline

Titanium oxide

Photodegradation

Semiempirical method

Model calculations

## ABSTRACT

In this work, a computational technique based on semiempirical SCF MO method MSINDO, has been used for the investigation of adsorption and initial oxidation step for the photodegradation of aniline on anatase  $\text{TiO}_2$  (100) surface. This surface has been chosen because it is present in  $\text{TiO}_2$  powders used in the adsorption experiments. Molecular dynamics (MD) simulations for the adsorption behavior of aniline have revealed a planar orientation of the aromatic ring to the surface linked via amino nitrogen with the surface lattice titanium ion. With the intention of predicting the primary photochemical and photocatalytic  $\cdot\text{OH}$  initiated oxidation intermediates, two different theoretical approaches, frontier electron theory and Wheland localization theory, have been applied. Based on our results, all isomers, *para*-, *ortho*- and *meta*-hydroxyaminocyclohexadienyl radicals, could be present in the case of photochemical oxidation, but the *para*- and *ortho*-positions are energetically more favorable than *meta*-position. Whereas, for the photocatalytic oxidation, where the aniline is adsorbed onto the  $\text{TiO}_2$  surface via amino group, the *para*- and *meta*-isomers are energetically more stable than the *ortho*-isomer, which is mainly influenced by steric hindrance.

© 2009 Elsevier B.V. All rights reserved.

## 1. Introduction

Aniline has been extensively studied because of its technological application in a vast amount of industrial processes [1]. It is known to be one of the more toxic pollutants released as effluents of several industries, and has been recognized as a high priority pollutant [2–4]. The heterogeneous photocatalysis of aniline in the presence of a semiconductor has become of significant interest over the last few decades [5,6]. Many semiconductor materials; namely  $\text{ZrO}_2$  [7],  $\text{CdS}$  [8],  $\text{Fe}_2\text{O}_3$  [9] and  $\text{TiO}_2$  [2], have been tested as photocatalysts for aniline oxidation, but it is generally accepted that  $\text{TiO}_2$  is the most reliable material [10]. The hydroxyl radical,  $\cdot\text{OH}$ , is regarded as the major species responsible for the degradation of organic pollutants, supported by experimental results from irradiated  $\text{TiO}_2$  suspensions [11,12].

Extensive experimental [7,8,13] and theoretical investigations [14] have focused on elucidating the structure [14] and photocatalysis [7,8,13] of aniline. However, various articles have dealt with the adsorption of aniline. In a photocatalytic degradation study of aniline at the interface of  $\text{TiO}_2$  suspensions containing carbonate ions, Kumar and Mathur [2] have observed increased intensity in the adsorption of aniline. This in turn results in increased interfa-

cial interaction of the photogenerated charge carriers with the adsorbed aniline and thus enhances its decomposition rate. Further, the adsorption and photodegradation of aniline and *N,N*-dimethyl-aniline, in acidic and alkaline media, has been examined by Canle et al. [15], using three  $\text{TiO}_2$  powders; anatase, rutile and Degussa P25. They concluded, on the one hand, that the pH of the medium is critical for the adsorption of both organic molecules and on the other hand, their results indicated that the main interaction between aniline and *N,N*-dimethyl-aniline and the surface of the catalyst takes place through the non-bonding electron pair of the amino group. The role of increase of adsorption on the degradation rate of *p*-aminophenol and *o*-aminophenol on  $\text{TiO}_2$  has been observed by Kamble et al. [16]. The former species have lower steric hindrance and adsorb to a greater extent on the semiconductor surface.

Finally, Palmisano et al. [17], in their work concerning the partial oxidation of aromatic compounds, including phenylamine in heterogeneous photolysis, concluded that the adsorption of the substrates onto the  $\text{TiO}_2$  surface is a relevant factor to be considered in the formation of the mono-hydroxy derivatives.

In order to deepen our understanding in the photochemical and photocatalytic oxidation of aniline by  $\cdot\text{OH}$  on  $\text{TiO}_2$ , we employ here a computational method to simulate the adsorption modes of aniline and probe their role in the initial steps of the oxidation process. The method is presented briefly in the next section and the obtained results follow. First, we have determined two modes of

\* Corresponding author. Present address: University of Technology, School of Applied Sciences, P.O. Box 35319, Baghdad, Iraq. Tel.: +964 7801 620 707.

E-mail addresses: [hswahab@yahoo.com](mailto:hswahab@yahoo.com), [hswahab@gmail.com](mailto:hswahab@gmail.com) (H.S. Wahab).

adsorption of aniline on TiO<sub>2</sub> and calculated their electronic and structural characteristics. Subsequently, we studied the primary photochemical oxidation of aniline in the gas phase by ·OH and obtained the possible products. Further, starting from the most stable structure of aniline–TiO<sub>2</sub> complex, which had been derived in advance, we probed the relevant pathways of the primary photocatalytic oxidation of aniline. Finally, in the conclusions we summarize our results.

## 2. Computational method

The quantum chemical model calculations are performed with the semiempirical MO method MSINDO, which is extensively documented for the first, second row main group elements [18,19] and the first row transition elements [20]. The transition metal atoms are described by a pseudo-minimal Slater basis set (3d,4s,4p) and the second row elements have a (2s,2p) basis set with different Slater exponents for intra- and inter-atomic integrals comparable to the Pople 6-31G basis set. Inner shells are taken into account by a pseudo potential after Zerner [21]. Molecular dynamics (MD) has been used for the studying of the dynamics of certain TiO<sub>2</sub>–C<sub>6</sub>H<sub>5</sub>NH<sub>2</sub> models, in which the average kinetic energy of the system becomes constant when simulation has reached constant temperature. Constant temperature dynamics are performed using Nosé–Hoover–Chain (NHC) thermostat.

The first step in the computational approach was to perform the full optimization for all the geometries of the isolated systems, substrates and clusters, and of the cluster–substrate complex. The molecular orbital calculations were carried out by a self-consistent field (SCF) method whose convergence criterion used throughout the calculations was an energy change below 10<sup>–9</sup> Hartree.

The next step in the computational analysis was to calculate the adsorption energies ( $E_{\text{ads}}$ ) for different adsorption modes from the quantum chemical total energies of the cluster–substrate system,  $E^{\text{cluster-substrate}}$ , the substrate,  $E^{\text{substrate}}$  and the cluster,  $E^{\text{cluster}}$  according to the following expression [22]:

$$E_{\text{ads}} = E^{\text{cluster-substrate}} - (E^{\text{substrate}} + E^{\text{cluster}}) \quad (1)$$

A negative value for  $E_{\text{ads}}$  therefore, designates a stabilization of the cluster–substrate system due to adsorption.

The vibrational frequencies and heats of formation are calculated using the keyword NVIB = 4 FULL, which is available in the framework of MSINDO [23], while, the energies and coefficients of the highest occupied molecular orbital (HOMO) and the lowest unoccupied molecular orbital (LUMO), are computed through the MOVEC keyword.

We have employed the saturated Ti<sub>36</sub>O<sub>90</sub>H<sub>36</sub> cluster model for modeling of anatase TiO<sub>2</sub> (100) surface, and further use it in the adsorption study. We followed similar water saturation strategy, for the coordinative unsaturated sites, reported in a previous study [24]. Moreover, this relatively small cluster is utilized in order to avoid excessive computer time in the subsequent adsorption calculations.

## 3. Results and discussion

### 3.1. Adsorption modes

The considered anatase TiO<sub>2</sub> (100) surface consists of five-fold coordinated titanium Ti<sub>5C</sub> atoms, Lewis acid sites, and two- and three-fold coordinated oxygen O<sub>2C</sub> and O<sub>3C</sub> atoms, Lewis base sites, whereas, the (100) × (010) edge implies other Lewis acid sites, which are the Ti atoms of four-fold coordinated titanium Ti<sub>4C</sub> (Fig. 1). This surface has been chosen because it is present in

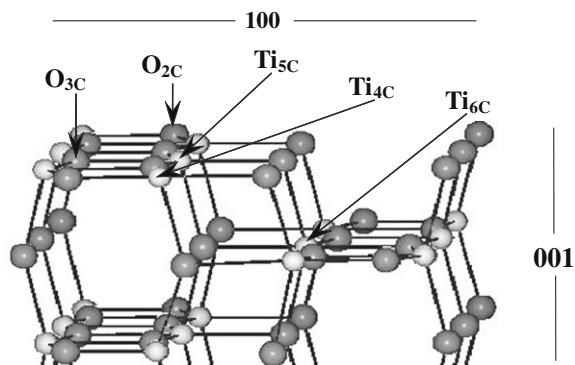


Fig. 1. The features of anatase TiO<sub>2</sub> (100) surface. Light spheres represent titanium atoms and the dark spheres represent oxygen atoms.

TiO<sub>2</sub> powders used in the adsorption experiments [25] and further, its crystallographic plane is isostructural with that of TiO<sub>2</sub> (010) surface [25,26]. Moreover, Martra [27] has concluded in a spectroscopic examination for two anatase powders, that anatase TiO<sub>2</sub> exposes mainly (001) and (100) surfaces with strong Lewis acid five-fold coordinated titanium atoms.

The optimization of the aniline geometry yields C–N and N–H bond distances of 1.394 and 0.997 Å, respectively. These values are in agreement with experimental results (1.402 and 1.001 Å) determined from microwave spectra [28], as well as with theoretical results (1.390 and 1.009 Å), obtained through B3LYP–DFT calculations with a 6-311++G\*\* basis set [29].

In the following, we examine, by means of MD simulations, the approach and adsorption of aniline on the TiO<sub>2</sub> (100) surface that lead to two different conformations starting from two initial arrangements, one parallel and one perpendicular to the surface. In the first case, the final conformation is depicted in Fig. 2.

The simulation starts from a non-optimized geometry to facilitate the crossing of any energy barriers. In the starting structure, the time step of the simulation is 1 fs. The aniline molecule approaches the surface resulting in closeness between the nitrogen atom and the surface lattice, i.e., the lone pair in nitrogen atom is pointing towards four-fold coordinated rather than five-fold coordinated titanium ion, and the initial parallel conformation is preserved. Vasudevan and Stone [30] have stated that, because of the high charge-to-radius ratio of Ti(IV) Lewis acid, the ionic contribution toward bonding is predominant for all Ti(IV)–organic ligand complexes. Furthermore, a small covalent contribution to bonding can exist because the Ti(IV) lowest unoccupied molecular orbital, LUMO (the empty d orbital), can accept electrons from the ligand. The same trend was observed with perpendicular adsorption model, which is illustrated in Fig. 3. In this case, the aniline molecule is oriented in parallel configuration to the surface due to optimization and further, linked via nitrogen atom to the surface lattice five-fold coordinated titanium ion.

The above findings, which envisage the dark adsorption of the substrate, indicate that the main interaction between aniline and the surface of TiO<sub>2</sub> takes place through the nitrogen of the amino group. This conclusion is in good accordance with the results of Canle et al. [15], who reported that the preliminary adsorption of aniline and *N,N*-dimethyl-aniline, in the dark, reached equilibrium concentration in one hour, and in addition, their interaction with TiO<sub>2</sub> surface is mediated through the amino group rather than via a  $\pi$ -interaction with the aromatic ring. Furthermore, Sanchez et al. [31], in their photocatalyzed destruction study for aniline in UV-illuminated aqueous TiO<sub>2</sub> suspensions, have observed a slight adsorption of aniline, in the dark, onto the TiO<sub>2</sub> surface, attaining

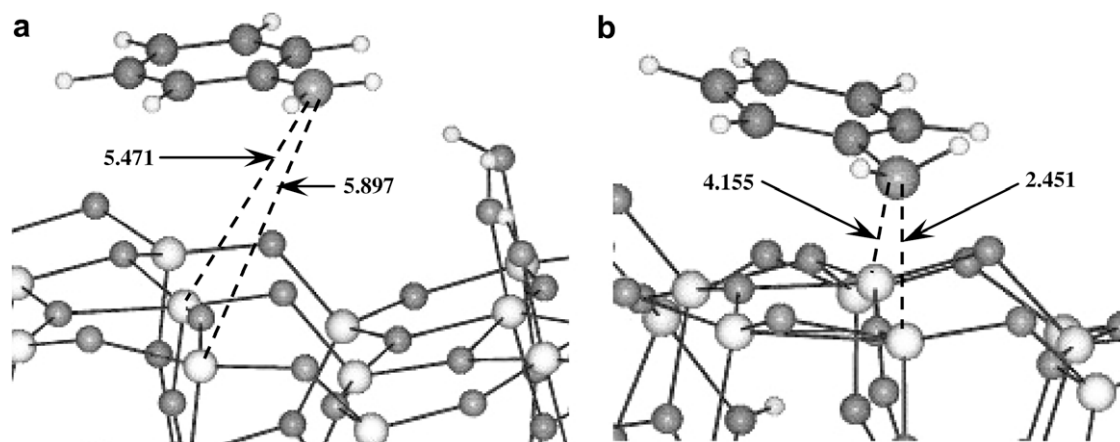


**Fig. 2.** MD simulation for parallel adsorption geometry: (a) initial structure; (b) minimum energy structure. Dashed lines represent distances. Ti (large light); H (small light); O (small dark); C (medium dark); N (large dark).

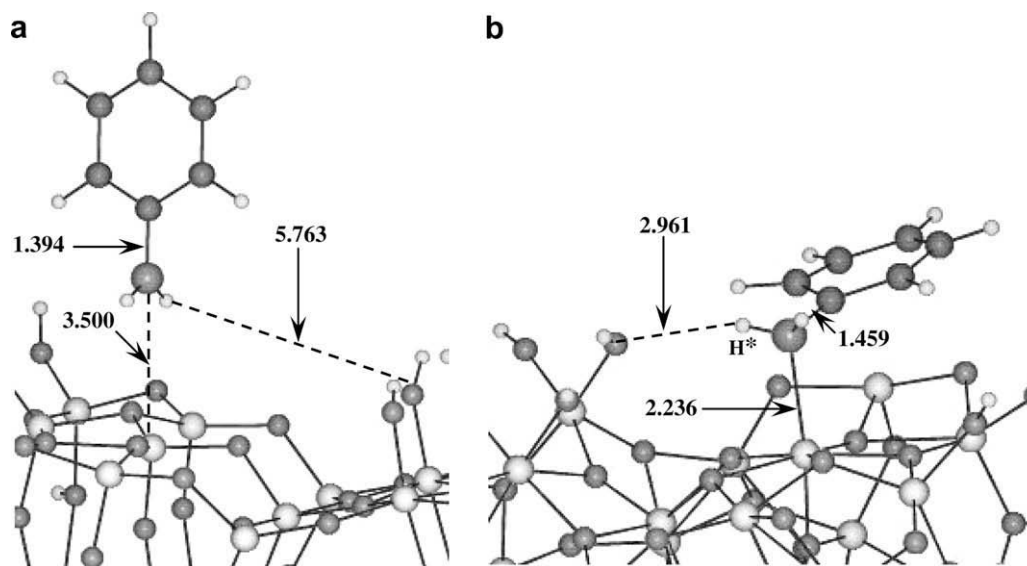


**Fig. 3.** MD simulation for perpendicular adsorption geometry: (a) initial structure; (b) minimum energy structure. Dashed lines represent distances. Ti (large light); H (small light); O (small dark); C (medium dark); N (large dark).

a limiting value of about 10% of the initial concentration after 10 min of contact.

Table 1 reveals the details of computed energies for the parallel and perpendicular adsorption systems. The lower binding energy (higher negative in magnitude) of the perpendicular adsorption conformation may highlight the possibility of its higher stability. Further, the higher dipole moment of perpendicular- over parallel-configuration refers to more polarity and consequently, higher stability.

From the data in Table 2, we notice that the Löwdin net charge values of amino nitrogen and surface titanium ion are less in the

case of perpendicular adsorption model, than those in the parallel adsorption model. This reveals explicitly the higher possibility of transfer, in the perpendicular geometry, for the non-bonding electron pair of nitrogen into the empty d orbital of Ti. This expectation is confirmed by the shorter, 2.236 Å, N–Ti bond distance in the optimized perpendicular model of adsorption (Fig. 3b).

The adsorption process is exothermic [32] accordingly; all  $E_{\text{ads}}$  values in Table 2 are negative in sign. Various conclusions can be drawn from Table 2: (a) lower substrate–surface interaction energy corresponds to closer approach of aniline to the surface; (b) preferential perpendicular conformation is predicted, which is

**Table 1**  
Computed energies of the parallel and perpendicular adsorption systems.

Energies	Aniline	Ti <sub>36</sub> O <sub>90</sub> H <sub>36</sub>	Parallel adsorption	Perpendicular adsorption
$E(\text{total})$ , a.u.	−49.1887	−1579.1271	−1628.3865	−1628.3928
Zero point energy, a.u.	0.1259	0.9187	1.0456	1.0460
$E(\text{total})$ , corrected, a.u.	−49.0628	−1578.2084	−1627.3409	−1627.3468
Binding energy, a.u.	−2.4570	−34.2838	−36.8114	−36.8177
Dipole moment, Debye	1.4110	2.8704	7.0988	7.8494

**Table 2**  
Characteristics of aniline adsorption modes on anatase TiO<sub>2</sub> (100) surface.

Initial geometry	N-Ti bond (Å)	N charge (a.u.)	Ti charge (a.u.)	$E_{\text{ads}}$ (a.u.)
Parallel	2.451	-0.3990	+1.2703	-0.0697
Perpendicular	2.236	-0.3123	+1.2052	-0.0756

energetically more favorable, with the amino nitrogen of aniline pointing towards the TiO<sub>2</sub> surface. This perpendicular conformation, as being more stable, is chosen for the subsequent adsorption studies.

For further analysis, we compute the vibrational density of states (VDOS) for the model seen in Fig. 3b, together with the free (non-adsorbed) aniline molecule (as a reference). The estimated VDOS for the reference aniline molecule and the selected atoms in the adsorption model are presented in Fig. 4a and b, respectively. The spectrum shown in Fig. 4a includes several bands located at 1060, 1300, 1650 and 3400 cm<sup>-1</sup>, which are assigned to aniline molecule. The band located at 1060 cm<sup>-1</sup> can be assigned to the amino N-H rocking vibration, the band at 1300 cm<sup>-1</sup> to the

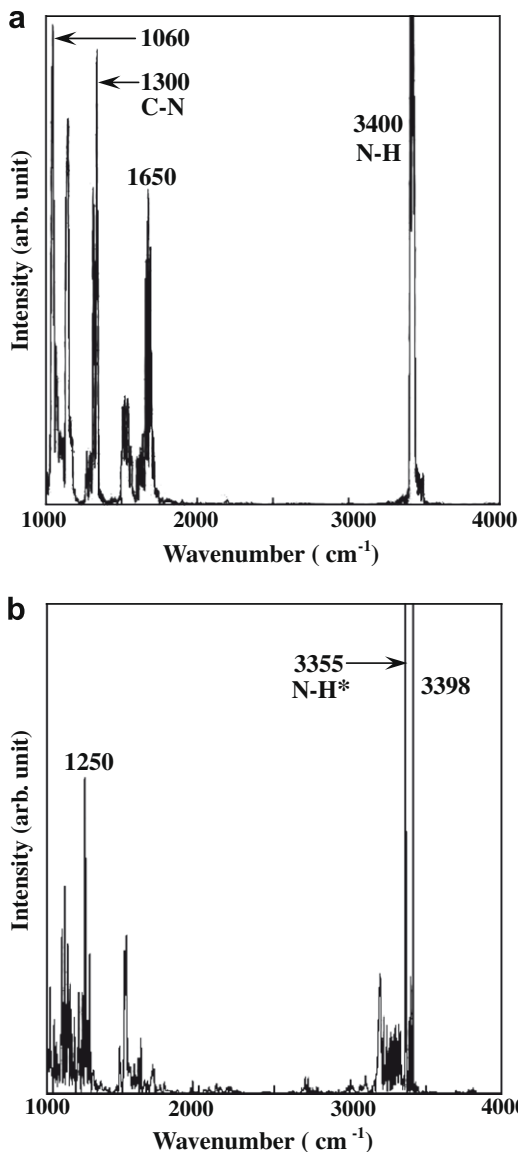


**Fig. 4.** The VDOS of aniline molecule adsorption on TiO<sub>2</sub> (100) surface: (a) VDOS of free aniline molecule as a reference; (b) VDOS of the adsorbed aniline molecule.

C-N in-plane stretching vibration, the band at 1650 cm<sup>-1</sup> to the N-H scissoring vibration, and the band at 3400 cm<sup>-1</sup> to the symmetric N-H stretching vibration. Similar bands located at 1050, 1276, 1619 and 3418 cm<sup>-1</sup> were observed for aniline experimentally [33]. Furthermore, from the ab initio MO calculations for aniline, using HF/6-31+G\* level of theory [34], analogous bands 1036, 1248, 1659 and 3407 cm<sup>-1</sup> have been also reported. A study of the spectrum seen in Fig. 4b reveals evidently a shift in C-N band and appearance of a new band located at 3355 cm<sup>-1</sup>. A major change in the spectrum (Fig. 4b) relative to that of the reference aniline spectrum (Fig. 4a) involves a shift in the amino C-N stretching vibration. This shift and the accompanying lowering of the corresponding intensity could be attributed to the weakening of the bond upon adsorption, in accordance with the lengthening of the C-N bond distance (Fig. 3b). Moreover, on the account of adsorption, two sets of peaks have appeared around 3355 and 3398 cm<sup>-1</sup> (Fig. 4b), which consequently indicates the existence of two types of hydrogen atoms. Although the hydrogen atoms of the amino group are similar, the type H\* hydrogen atom (Fig. 3b) has shown some sort of a red-shift in its stretching frequency, which could be due to hydrogen bonding with the oxygen of the boundary hydroxyl group. Accordingly, the adsorbed amino group exhibits two different types of hydrogen atoms due to the difference in their bonding features. In conclusion, the predicted VDOS spectra indicate that aniline molecules are adsorbed to the surface through the amino group.

### 3.2. Photochemical oxidation

We proceed with the study of the approach of ·OH to the free aniline. Already it has been reported that ·OH radical [15] is regarded as the major species responsible for the degradation of organic pollutants. Furthermore, from the determination of intermediate compounds generated during the first oxidation steps, mechanistic studies have shown that ·OH radicals are the species involved in the oxidation processes [17] which consequently, lead to the formation of hydroxycyclohexadienyl radicals [15].

There are several theoretical approaches in the literature for the determination of the primary oxidation interaction sites of ·OH radical with aromatic molecules through addition, to yield hydroxycyclohexadienyl type radical [35]. One of the highly successful ones is the “frontier electron theory”, which states that in electrophilic reactions, the point of interaction should be at the position of greatest electron density in the HOMO of a molecule, whereas in the nucleophilic interaction, the attack is expected at the position where LUMO has the maximum electron density [36]. Another theory which has also been very successful is the Wheland localization approach [37]. In this theory, the position of attack is assigned by the energy of the Wheland intermediates.

The HOMO and LUMO energy levels of aniline and singly occupied molecular orbital (SOMO) of the ·OH radical are schematically represented in Fig. 5. From this figure one can foresee that in the hydroxylation of aniline, the interaction of the SOMO (-0.5493 a.u.) of ·OH radical with HOMO (-0.2771 a.u.) of aniline predominates, since the ·OH radical has a very low-lying SOMO. Whereas, the SOMO/LUMO interactions, i.e., electron transfer from ·OH radical to the LUMO of aniline, would require high activation energy. The HOMO coefficients for the aniline molecule obtained in this study are shown in Fig. 6a. The values of the coefficients for the photochemical oxidation, i.e., homogeneous photolysis, indicate the preference of the reactivity sequence as *para*->*ortho*->*meta*-positions with respect to the functional -NH<sub>2</sub> group. Also from Fig. 6a, one can notice the large HOMO coefficients at the nitrogen (N) and the substituted carbon (C1) atoms. This would

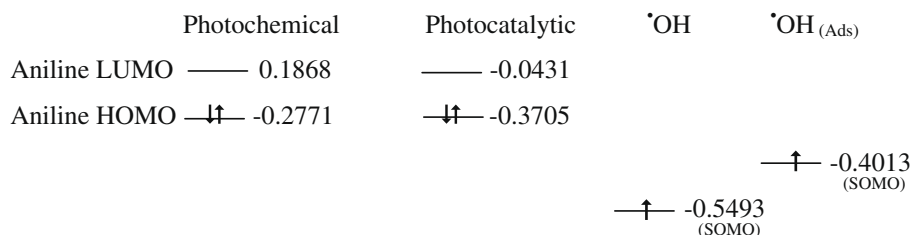


Fig. 5. HOMO–LUMO and SOMO energies, in atomic units, for aniline and hydroxy group radical, respectively.

lead one to expect the attack of  $\cdot\text{OH}$  radical is either on N or C1 atom. At the substituted carbon atom, there is a steric hindrance which may cause an increase in the activation energy of the interaction. On the other hand, there is experimental evidence that  $\cdot\text{OH}$  radicals attack aromatic molecules at the ring positions [35].

With the aromatic skeleton remaining unchanged during the calculations for the free (non-adsorbed) monohydroxyaminocyclohexadienyl radicals, we have obtained energies, and thus the relative stability of the species, as well as heats of formation, as presented in Table 3. In line with Wheland approach and from the data shown in Table 3, it could be concluded that the stability of the Wheland intermediates follows the sequence of *para*->*ortho*->*meta*-hydroxyaminocyclohexadienyl radical, although the energy differences are small. Thus, both frontier electron theory and Wheland approach predict similar reactivity sequence, with the *para*-position being predominant. The stability of *para*- and *ortho*-hydroxylated radicals over *meta*-ones, is mainly ascribed to the resonance structures, in which the unpaired electron of the radical is on the carbon bonded to the electron donating group –NH<sub>2</sub> [17]. These resonance structures can exist only when hydroxyl radical enters *para*- and *ortho*-positions.

Another interesting result is that the SOMO energy of the *meta*-adduct is lying below the corresponding energies of the *ortho*- and *para*-adducts, Table 3. This observation is in accordance with the results of Eberhardt and Yoshida [36] for the hydroxylation of toluene. They report that due to the selectivity in the disproportion-

ation, the *m*-hydroxymethylcyclohexadienyl radical adduct acts preferentially as oxidizing species in disproportionation reactions.

### 3.3. Photocatalytic oxidation

After ensuring the description of the oxidation of free aniline by the  $\cdot\text{OH}$  radical through the present method, we proceed to analyze the catalytic degradation of adsorbed aniline. As in the previous case, the SOMO (–0.4013 a.u.) of the  $\cdot\text{OH}$  radical lies close to the HOMO (–0.3705 a.u.) of the adsorbed aniline, Fig. 5, revealing the possibility of heterogeneous photolysis on the TiO<sub>2</sub> surface. The average values of the HOMO coefficients, which are presented in Fig. 6b, for the *ortho*- (C2 and C6), *meta*- (C3 and C5) and *para*- (C4) positions, of the adsorbed aniline molecule (Fig. 3b) on the photocatalyst surface, with respect to the functional –NH<sub>2</sub> group, indicate a variation in the priority sequence of  $\cdot\text{OH}$  radical attack, in comparison to the homogeneous photolysis, with domination of *ortho*- and *meta*- over *para*-orientations. Whereas, the computation of the total energies and heats of formation for the adsorbed hydroxyaminocyclohexadienyl radical intermediates, has exhibited (Table 3) comparable values with preference for the *para*- and *meta*- over *ortho*-conformations. Hence, notwithstanding of higher HOMO coefficients for *ortho*-position, both *para*- and *meta*-positions result in more stable intermediates, i.e., the frontier electron theory and localization approach do not give the same predictions.

This result in the hydroxylation of adsorbed aniline could be explained in the following manner: the frontier electron theory predicts the position of initial interaction, whereas by Wheland approach the thermodynamic favorability of the produced radical intermediates, upon initial oxidation, is ensured. This would lead one to postulate that although frontier electron theory correctly predicts the position of initial attack, it may not reflect adequately the distribution of the isomers. Furthermore, the adsorption configuration (Fig. 3b) reveals obviously the closeness of *ortho*-position to the surface more than *meta*- and *para*-positions, which are pointed farther away from the surface. This could preclude, i.e., lower rate, the initial  $\cdot\text{OH}$  mediated oxidation of *ortho*-position. Apart from that, the *ortho*-position has already more steric hindrance, due to the adsorbed amino group, in comparison to *meta*- and *para*-positions. Kamble et al. [16] have observed, in their photocatalytic degradation of aniline, the predominance of *o*-aminophenol intermediate in the bulk, since adsorption onto the

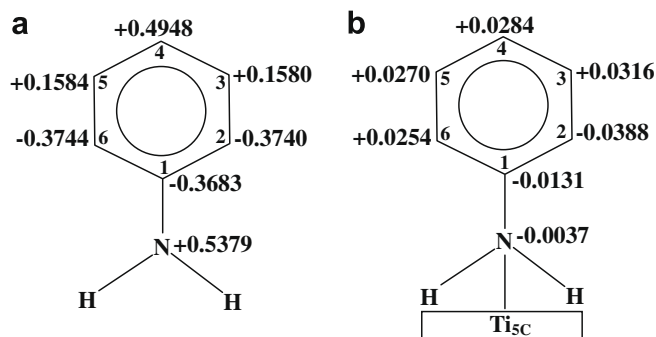


Fig. 6. HOMO coefficients for: (a) free aniline; (b) adsorbed aniline onto TiO<sub>2</sub> surface.

Table 3  
MSINDO calculations on free and adsorbed hydroxyaminocyclohexadienyl radicals.

Parameter	<i>ortho</i>		<i>meta</i>		<i>para</i>	
	Free	Absorbed	Free	Absorbed	Free	Absorbed
$E(\text{total})$ , a.u.	–65.5905	–1644.898	–65.5895	–1644.902	65.5913	–1644.906
$\Delta E$ , kJ/mol	2.100	21.000	4.725	10.500	0.000	0.000
$\Delta H_f$ , kJ/mol	–66.88	–41544	–63.95	–41558	–68.97	–41569
$E(\text{SOMO})$ , a.u.	–0.2643	–0.3310	–0.3054	–0.3355	–0.2622	–0.3277

surface is influenced by the steric hindrance. Whereas, Palmisano et al. [17] have reported, for the heterogeneous photocatalysis of some aromatic compounds containing electron donating groups, that the main mono-hydroxylated compounds were *ortho*- and *para*-isomers and the *meta*-isomer was also present but in small amounts.

Based on the above results, the differences in the isomer distribution pattern, i.e., the reactivity of *para*-, *meta*- and *ortho*-positions, for the photocatalytic oxidation of aniline molecule in comparison to that for photochemical oxidation could be ascribed mainly to the adsorption process. Canle et al. [15] have reported that at  $\text{pH}_{\text{ads}}$  ( $3.5 < \text{pH} < 5.5$ ), the interaction between the slightly positively charged  $\text{TiO}_2$  surface and the non-bonding electron pair of the nitrogen is optimal. As a result, one may postulate that the delocalization of non-bonded electron pair into the aromatic system would be much less due to the adsorption. We can therefore, hypothesize that the variation of charge distribution over the benzene ring and consequently modifications in the reactivity of  $\cdot\text{OH}$  radical attacking positions are possible. As can be seen from the results in Table 3, the SOMO of adsorbed *m*-hydroxyaminocyclohexadienyl radical is lying again, as in the case of photochemical oxidation, lower than both *para*- and *ortho*-orientations. This result is in good agreement with the experimental and theoretical observations of Eberhardt and Yoshida [36] for the hydroxylation of toluene.

On the basis of these results and from the mechanistic point of view, it could be inferred that the photoproducts extracted from the  $\text{TiO}_2$  surface after the photoprocess, and detected experimentally, may not reflect the actual species that are formed on the surface during the illumination process. Accordingly, the characterization of the photooxidation intermediate products is useful source of information for the organic pollutants photo oxidative degradation pathways.

#### 4. Conclusions

We have shown through MSINDO molecular calculations that the adsorption of aniline onto  $\text{TiO}_2$  surface starting from perpendicular configuration is more favored energetically than that started from parallel configuration. The optimization of the initial conformations of aniline have produced two planar structures of different stability, with aniline molecule linked to the lattice Ti ion through the amino nitrogen. Such structures, therefore, are expected to influence the formation of mono-hydroxy intermediates during the degradation of adsorbed aniline. In the case of photochemical oxidation, all the isomers could be present, but the *para*- and *ortho*-positions are energetically more favorable than *meta*-position toward  $\cdot\text{OH}$  radical attack. However, in the case of the photocatalytic oxidation, the behavior exhibited is quite different due to the adsorption of aniline onto the  $\text{TiO}_2$  surface through the amino group. This attachment introduces steric hindrance on the *ortho*-position of the aromatic ring and makes it less favored for an  $\cdot\text{OH}$  attack. The observed stabilities, although found to lie close to each other, are in accordance with this observation

predicting a decreasing preference of attack in the sequence of *para*-, *meta*- and *ortho*-positions.

#### Acknowledgments

One of the authors (H.S. Wahab) warmly thanks the Greek Ministry of Education and Religious Affairs for the award of a research fellowship and the International Institute of Education/SRF for supporting a postdoctoral stay. This work was partially supported by a grant from the Research Account of the National and Kapodistrian University of Athens (No. 70/4/6482). The constructive and useful comments of the referees are also acknowledged.

#### References

- [1] M.E. Vaschetto, B.A. Retamal, A.P. Monkman, J. Mol. Struct. (THEOCHEM) 468 (1999) 209.
- [2] A. Kumar, N. Mathur, J. Colloid Interf. Sci. 300 (2006) 244.
- [3] S.V. Kotelevtsev, O.O.P. Hanninen, P.A. Lindström-Seppa, S.E. Huskon, L.I. Stepanova, V.M. Glaser, A.M. Beim, Aquat. Ecosyst. Health Manage. 3 (2000) 95.
- [4] United States Environmental Protection Agency, OPPT Chemical Fact Sheets, Aniline Fact Sheet; Support Document (CAS No. 62-53-3), December 1994.
- [5] D.F. Oills, Environ. Sci. Technol. 19 (1985) 480.
- [6] P.V. Kamat, Chem. Rev. 93 (1993) 267.
- [7] C. Karunakaran, S. Senthivelan, J. Mol. Catal. A: Chem. 233 (2005) 1.
- [8] C. Karunakaran, S. Senthivelan, Sol. Energy 79 (2005) 505.
- [9] C. Karunakaran, S. Senthivelan, Electrochem. Commun. 8 (2006) 95.
- [10] A. Fujishima, K. Hashimoto, T. Watanabe,  $\text{TiO}_2$  Photocatalysis, Fundamentals and Application, BKC Inc., Tokyo, 1999.
- [11] P.F. Schwarz, N.J. Turro, S.H. Bossmann, A.M. Braun, A.M.A.A. Wahab, H. Dürr, J. Phys. Chem. B 101 (1997) 7127.
- [12] Y. Nosaka, Y. Yamashita, H. Fukuyama, J. Phys. Chem. B 101 (1997) 5822.
- [13] W.B. Tzeng, K. Narayana, J. Mol. Struct. (THEOCHEM) 434 (1998) 247.
- [14] Y. Wang, S. Saebø, C.U. Pittman Jr., J. Mol. Struct. (THEOCHEM) 281 (1993) 91.
- [15] M.L. Canle, J.A. Santaballa, E. Vulliet, J. Photochem. Photobiol. A 175 (2005) 192.
- [16] S.P. Kamble, S.B. Sawant, J.C. Schouten, V.G. Pangarkar, J. Chem. Technol. Biotechnol. 865 (2003) 78.
- [17] G. Palmisano, M. Addamo, V. Augugliaro, T. Caronna, A. Di Paola, E.G. Lopez, V. Loddo, G. Marci, L. Palmesano, M. Schiavello, Catal. Today 122 (2007) 118.
- [18] B. Ahlswede, K. Jug, J. Comput. Chem. 20 (1999) 563.
- [19] B. Ahlswede, K. Jug, J. Comput. Chem. 20 (1999) 572.
- [20] T. Bredow, G. Geudtner, K. Jug, J. Comput. Chem. 22 (2001) 861.
- [21] M.C. Zerner, Mol. Phys. 23 (1972) 963.
- [22] T. Homann, T. Bredow, K. Jug, Surf. Sci. 555 (2004) 135.
- [23] H.S. Wahab, T. Bredow, S.M. Aliwi, Chem. Phys. 353 (2008) 93.
- [24] H.S. Wahab, T. Bredow, S.M. Aliwi, J. Mol. Struct. (THEOCHEM) 868 (2008) 101.
- [25] A. Vittadini, A. Selloni, F.P. Rotzinger, M. Grätzel, Phys. Rev. Lett. 81 (1998) 2954.
- [26] A. Beltran, J.R. Sambrano, M. Calatayud, F.R. Sensato, J. Andres, Surf. Sci. 490 (2001) 116.
- [27] G. Martra, Appl. Catal. A 200 (2000) 275.
- [28] D.G. Lister, J.K. Tyler, J.H. Hog, N.W. Larsen, J. Mol. Struct. 23 (1974) 253.
- [29] A.K. Rai, S. Kumar, A. Rai, Vib. Spectrosc. 42 (2006) 397.
- [30] D. Vasudevan, A.T. Stone, Environ. Sci. Technol. 30 (1996) 1604.
- [31] L. Sanchez, J. Peral, X. Domenech, Electrochim. Acta 42 (1997) 1877.
- [32] N. Serpone, E. Pelizzetti, Photocatalysis, Fundamentals and Applications, John Wiley and Sons, New York, 1989.
- [33] J.C. Evans, Spectrochim. Acta 16 (1960) 428.
- [34] W.B. Tzeng, K. Narayanan, K.C. Shieh, C.C. Tung, J. Mol. Struct. (THEOCHEM) 428 (1998) 231.
- [35] N. San, A. Hatipoglu, G. Koçtürk, Z. Çınar, J. Photochem. Photobiol. A 146 (2002) 189.
- [36] M.K. Eberhardt, M. Yoshida, J. Phys. Chem. 77 (1973) 589.
- [37] G.W. Wheland, J. Am. Chem. Soc. 64 (1942) 900.